ADVANCED FUNCTIONAL MATERIALS
www.afm-journal.de

Preparation of Iron Networks Hosted in Porous Alumina with Tunable Negative Permittivity and Permeability

Zhi-cheng Shi, Run-hua Fan, Ke-lan Yan, Kai Sun, Meng Zhang, Cheng-guo Wang,* Xiang-fa Liu, and Xi-hua Zhang*

Random composites of iron particles hosted in porous alumina were prepared from a facile impregnation-reduction process. Interestingly, when the iron content exceeds the percolation threshold, the interconnection of iron particles results in the formation of iron networks. The composites then change from capacitive to inductive and the conductive mechanism changes from hopping conduction to metal-like conduction. The negative permittivity was attributed to the plasma oscillation of delocalized electrons in iron networks, while the negative permeability could be ascribed to the strong diamagnetic response of current loops in iron networks. The negative permittivity behavior of the iron/alumina composite was analyzed using Drude model. Additionally, the fitting results indicated that the effective plasma frequency of the iron/alumina composite is much lower than bulk iron. Further investigations show that, the iron content and reduction temperature can easily tune the amplitude and frequency ranges of the negative permittivity and permeability. Moreover, the negative permittivity region and the negative permeability region can be pushed to the same frequency region by adjusting the iron content and reduction temperature. The impregnation-reduction process opens a new way for the realization of tunable negative permittivity and permeability in random composites, and has great potential for the preparation of new types of double negative materials.

1. Introduction

In recent years, considerable attention has been paid to the development of materials with simultaneously negative permittivity and permeability, termed double negative materials (DNMs). They have unique electromagnetic properties and novel potential applications.[1–3] In 2000, Smith et al. successfully obtained double negative property in an artificial medium of periodic metallic wires and rings.[4] From then on, various metamaterials with arrays of periodic building blocks have been fabricated to achieve double negative property in the last few years.[5–9] Recently, switchable magnetic metamaterial was demonstrated via reshaping micromachined metamaterial molecules,[10] and metamaterials with tunable terahertz anisotropy were fabricated in periodic micromachined Maltese-crosses.[11] As is well known, metamaterials with periodic elements obtain their double negative property from the artificial periodic structures rather than directly from the materials' nature. It is worth noting that, Moreau et al. demonstrated a simple method to create metamaterials by randomly adsorbing chemically synthesized silver nanocube onto a nanometer-scale thick polymer spacer layer on a gold film.[12] Therefore, it is also interesting to investigate the possibility of realizing double negative property from the point of "real" random materials without periodic building blocks. These DNMs, so-called random composites for DNMs (RC-DNMs), can be prepared by typical processing of material, which make it possible to explore new DNMs and potential applications, and to feasibly tune their electromagnetic parameters by controlling their composition and microstructure. Based on the above, great efforts have been made to search for RC-DNMs in recent years. Although many "real" materials with single negative permittivity[13–15] or single negative permeability[16,17] have been reported, limited work has been made to obtain random composites with simultaneous negative permittivity and permeability.[18] Theoretically, it is possible to obtain double negative property in metallic magnetic granular composites.[19] In particular, Hur et al. theoretically predicated that DNMs could be fabricated using random composites containing three dimensional metallic networks.[20] The plasma oscillation of free electrons in metallic networks could generate negative permittivity. Meanwhile, the strong diamagnetic response of metallic networks could generate negative permeability.[21] Therefore, random composites containing metallic networks will be promising candidates for RC-DNMs.

Various methods have been reported for the preparation of metallic networks, such as templating, dealloying and laser etching.[22] However, how to introduce these metallic networks into a bulk matrix is still a problem to be solved. In our recent work,[23] random composites of nickel networks randomly hosted in porous alumina were prepared using a facile impregnation-reduction process. And simultaneous negative

Z.-C. Shi, Prof. R.-H. Fan, K.-L. Yan, K. Sun, M. Zhang, C.-G. Wang, X.-F. Liu, X.-H. Zhang
Key Laboratory for Liquid-Solid Structural Evolution and Processing of Materials (Ministry of Education)
Shandong University
Jinan 250061, China
E-mail: fan@sdu.edu.cn; wangchg@sdu.edu.cn

DOI: 10.1002/adfm.201202895

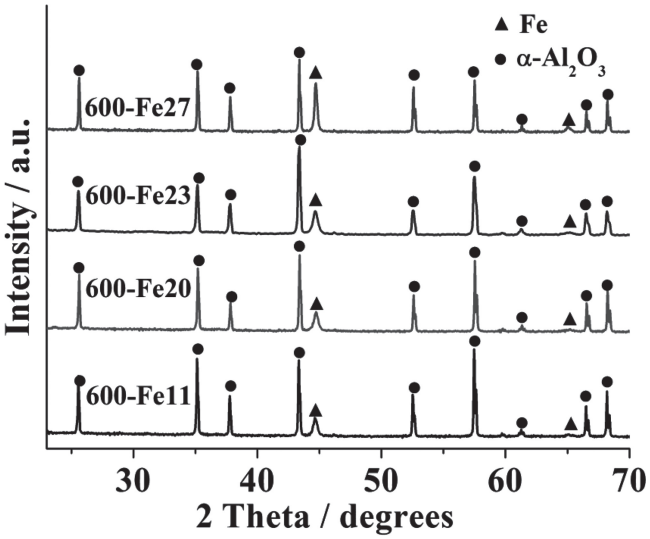

Figure 1. XRD patterns of the composites with different iron contents.

permittivity and permeability were obtained. However, how to adjust the negative permittivity and permeability by preparation processes is still a meaningful subject to be further investigated. In the present work, iron networks were hosted in porous alumina via the impregnation-reduction process which includes three steps: impregnation, calcination, and reduction. The main text of this paper includes two parts. In the first part, the composition, microstructure, and electromagnetic properties of the Fe/Al_2O_3 composites reduced at 600 °C are discussed. Interestingly, negative permittivity and negative permeability appeared in the composites with iron contents of 20, 23, and 27 wt%. For the composites with iron content of 20 and 23 wt%, negative permittivity and negative permeability were obtained at different frequency regions. Fortunately, when the iron content reaches 27 wt%, the negative permittivity region overlaps with the negative permeability region from ~750 MHz to ~1 GHz. In the second part, the reduction temperatures were further reduced to 500 °C, 400 °C, 300 °C and 250 °C to investigate how to control the frequency regions of negative permittivity and negative permeability as well as how to push the negative permeability and permittivity towards the same frequency region.

2. Results

2.1. Characterization, and Dielectric and Magnetic Properties of the Composites Prepared at 600 °C

The X-ray Diffraction (XRD) patterns of the composites (reduction temperature is 600 °C) shown in **Figure 1** indicate that the composites consist of iron and alumina, without any additional phases. The Scanning Electron Microscope (SEM) images of Fe/Al_2O_3 composites are shown in **Figure 2**. Isolated iron particles with typical size of ≈100 nm are homogeneously distributed in porous alumina for sample 600-Fe11 (see the Experimental Section; reduction temperature: 600 °C, iron content: 11 wt%). Further increasing the iron content leads to the interconnection of iron particles, and iron networks were formed when iron content reaches 23 and 27 wt%. The interconnectivity enhancement of iron particles with increasing iron content can also be verified by the ac conductivity σ_{ac}. As shown in **Figure 3**, the

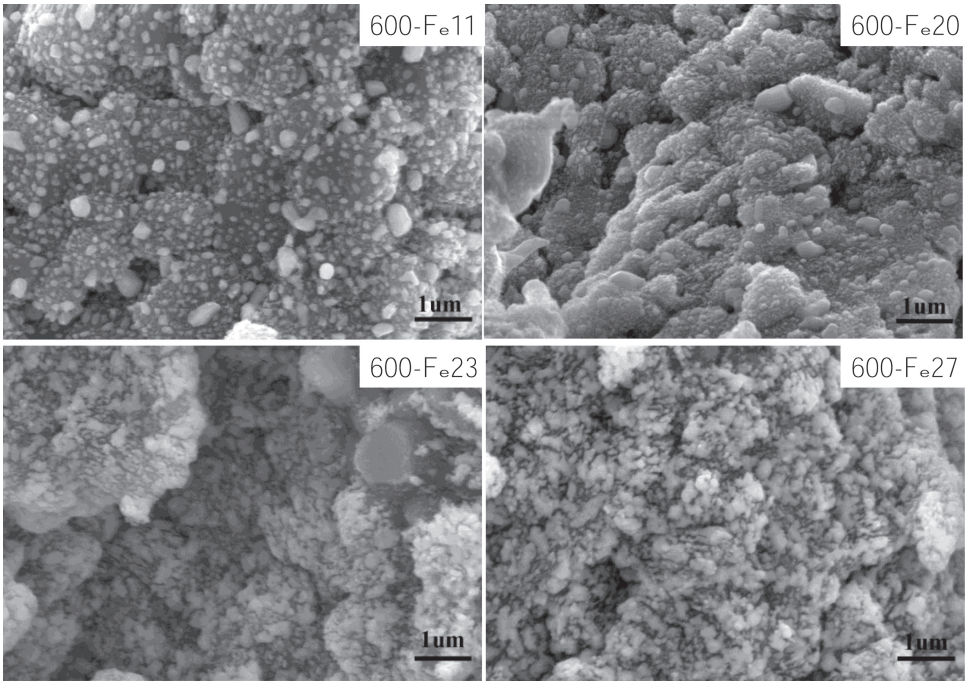

Figure 2. SEM images of the composites with different iron contents. Increasing the iron content leads to the interconnection of iron particles, hence the formation of iron networks.

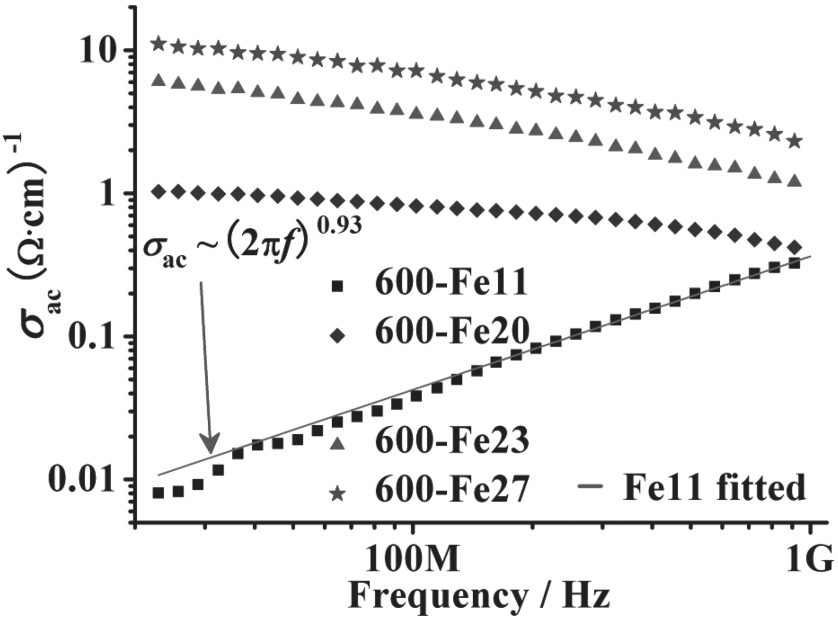

Figure 3. Frequency dependences of ac conductivity σac for composites with different iron contents. The conductive mechanism of 600-Fe11 is hopping conduction which follows the power law $\sigma_{ac} \approx (2\pi f)^{0.93}$, while 600-Fe20, 600-Fe23 and 600-Fe27 are metal-like conduction due to the formation of iron network.

ac conductivity σ_{ac} increases with iron content. In particular, the σ_{ac} increases considerably for 600-Fe20 compared with 600-Fe11, which could be attributed to the percolation behavior due to the formation of iron networks throughout the composite.[24] Moreover, the frequency dependence of σ_{ac} varies with increasing iron content. As shown in Figure 3, the σ_{ac} of 600-Fe11 increases with increasing frequency, and the σ_{ac} is proportional to the frequency. Further analysis shows that the σ_{ac}–f relationship follows the power law $\sigma_{ac} \approx (2\pi f)^{0.93}$ characterizing hopping conduction.[25] For samples 600-Fe20, 600-Fe23 and 600-Fe27, σ_{ac} decreases with increasing frequency which should be attributed to the skin effects.

The frequency dependences of permittivity for composites prepared with a reduction temperature of 600 °C are presented in **Figure 4**a,c. Negative ε' is observed in the composites with high iron content (20, 23, and 27 wt%), while positive ε' is obtained in the composite with low iron content (11 wt%, **Figure 5**a). Moreover, the amplitude of negative ε' increases with increasing iron content (Figure 4a). Two fano-type resonances that switch ε' from negative to positive at ≈120 MHz and ≈60 MHz are observed in 600-Fe20 and 600-Fe23, respectively. Meanwhile, two corresponding dielectric loss peaks appear in Figure 4c. For 600-Fe20 and 600-Fe23, the iron contents exceed their percolation thresholds, leading to their inductive behaviors. Therefore, they could be equivalent of circuit models consisting of inductance L and capacitance C. L is determined by conductive electrons in iron networks,

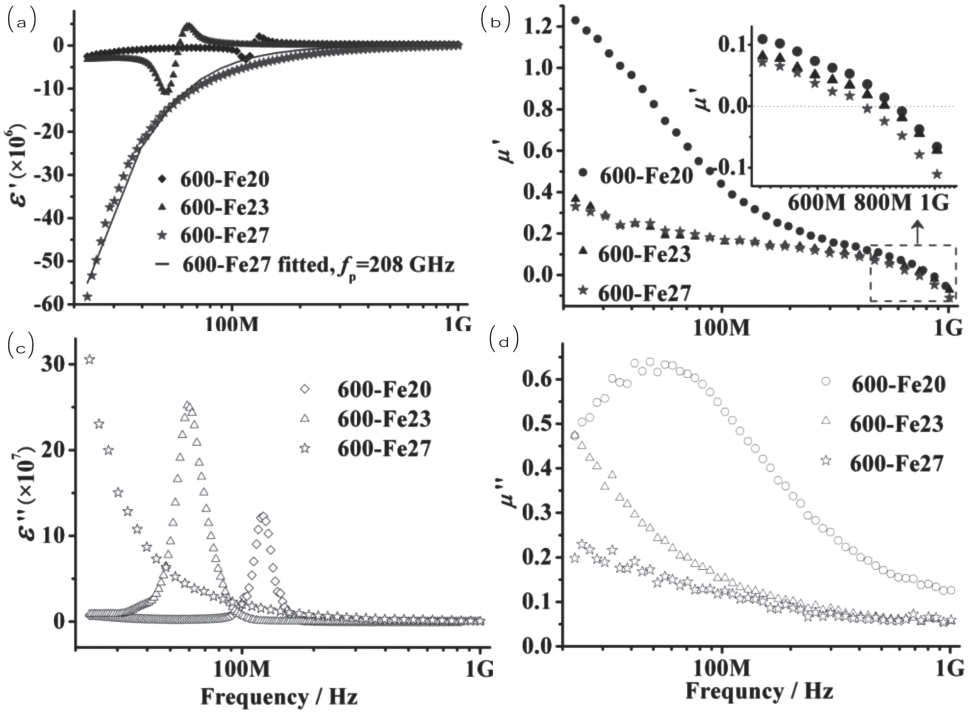

Figure 4. Frequency dependences of a,c) permittivity and b,d) permeability for composites with different iron contents. a) Negative permittivity and b) permeability with different amplitude and frequency ranges are observed. Two fano-type resonances that switches ε' from negative to positive at ≈120 MHz and ≈60 MHz are observed in 600-Fe20 and 600-Fe23, respectively. Fitted results by the Drude model for Fe27 is shown as the solid line in Figure 4a.

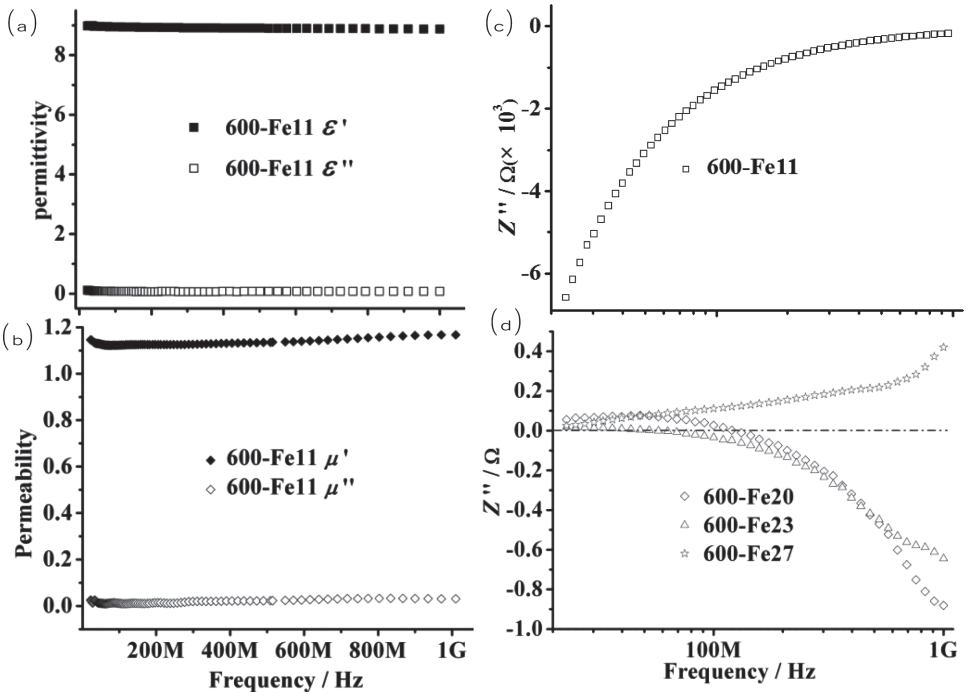

Figure 5. Frequency dependences of a) permittivity, b) permeability, and c,d) impedance for composites reduced at 600 °C. Fe11 manifests capacitive behavior ($Z''<0$, Figure 5c), while 600-Fe20, 600-Fe23 and 600-Fe27 manifest inductive behavior ($Z''>0$, Figure 5d). The interconnectivity level of iron particles in 600-Fe20, 600-Fe23 and 600-Fe27 exceeds some critical point, leading to the formation of current loops in iron networks. Then a lag of the current behind of the voltage occurs, which gives rise to the inductive behavior.

while C is determined by polarized electrons. As shown in Figure 5d, Z'' becomes zero at ≈120 MHz and ≈60 MHz for 600-Fe20 and 600-Fe23, respectively. And LC resonance will take place when Z'' becomes zero, leading to the emission of electromagnetic radiations. The LC resonance frequency (the emitted electromagnetic radiation frequency) is expressed as $f = 1/[2\pi(LC)^{1/2}]$. Iron content will influence the values of L and C, hence the frequency of emitted electromagnetic radiations. When the emitted electromagnetic radiations interfere with the external high frequency electric field, the fano-type frequency dispersion takes place. Further increasing the iron content to 27 wt% results in negative ε' in the whole tested frequency range (Figure 4a). The negative permittivity was considered to be resulted from the formation of continuous conductive pathways in the composites. Similar negative permittivity phenomenon was also reported in carbon nanofiber/polyetherimide composites[13,26] and polyaniline nano-composites.[27] Furthermore, the plasma-like negative permittivity behavior of 600-Fe27 was fitted using Drude model:[28] $\varepsilon_r'(\omega) = 1-\omega_p^2/(\omega^2+\omega^2)$, $\omega_p = [n_{eff}e^2/(m_{eff}\varepsilon_0)]^{1/2}$, where ω_p ($\omega_p = 2\pi f_p$) is the plasma frequency, ω frequency of electric field, ω_τ damping parameter, ε_0 permittivity of vacuum (8.85×10^{-12} F/m)′ n_{eff} effective concentration of delocalized electrons, m_{eff} effective weight of electron, and e electron charge (1.6×10^{-19} C). The ε' - f curve of 600-Fe27 fitted using Drude model (solid line in Figure 4a) agrees well with the experimental results, suggesting the effective f_p of 208 GHz. For bulk iron, the permittivity ε' is negative until its plasma frequency $f_p = \omega_p/2\pi = 3.66 \times 10^6$ GHz.[29] While for 600-Fe27, only part of the composite is filled with iron, leading to a dilution of the average concentration of electrons (a decrease of n_{eff}) as compared with bulk iron. In addition, electrons are constrained to move along iron thin networks, resulting in a considerable enhancement of m_{eff}.[30] Therefore, the effective plasma frequency of 600-Fe27 is much lower than that of the bulk iron according to Drude model.

The permeability spectra of composites with reduction temperature of 600 °C are presented in Figure 4b,d and Figure 5b. For samples 600-Fe20, 600-Fe23 and 600-Fe27, μ' decreases with increasing frequency due to the effect of magnetic resonances and eddy currents.[16] A magnetic loss peak corresponding to the decrease of μ' is observed for 600-Fe20 in Figure 4d. Magnetic loss peaks of 600-Fe23 and 600-Fe27 may also appear at lower frequencies which are beyond the tested frequency range in the present work. For sample 600-Fe11, the magnetic responses and eddy currents are very weak due to the low content of iron. Therefore, the μ' and μ'' of 600-Fe11 are almost independent of frequency (Figure 5b) in the tested frequency range. Interestingly, negative μ' is observed for 600-Fe20, 600-Fe23 and 600-Fe27 above 700 MHz. And the higher the iron content, the lower negative μ' is (inset of Figure 4b). For the permeability measurements, the Fe/Al_2O_3 rings (inner diameter, outer diameter and height were 6.5, 19, and 2 mm, respectively) were put into a short-ended coaxial line resonator. Then a high frequency electromagnetic signal was applied. That is to say, the iron networks were put into a high frequency electromagnetic field during the test process. Therefore, current loops will be induced in iron networks under the action of high frequency electromagnetic field. And the extra

electromagnetic field induced by the current loops will be opposite to the external high frequency electromagnetic field. Once the strong electromagnetic field induced by the current loops counterbalances or dominates the external magnetic field, the negative permeability behavior may occur.[21] Moreover, higher iron content enhanced the grid density of iron networks. And more current loops will be induced under high frequency electromagnetic field, leading to lower negative μ'.[21] Besides, the domain wall motion and gyromagnetic spin rotation may also contribute to the negative permeability behavior.[16] Furthermore, the negative μ' of Fe/Al_2O_3 composites in the present work may also become tunable by applying an external DC magnetic field.[14,31,32]

2.2. Dielectric and Magnetic Properties of the Composites Prepared with Different Reduction Temperatures

It is well recognized that the dielectric and magnetic properties of composites were closely related to their composition and microstructures. Therefore, a series of Fe/Al_2O_3 composites with reduction temperature of 500, 400, 300, and 250 °C were further prepared, respectively. And **Figure 6** shows the frequency dependences of conductivity for the composites. It is indicated that, higher iron content and higher reduction temperature lead to the increase of the ac conductivity. When the reduction temperature is 250 °C, the composites consist of Fe_3O_4, Fe_2O_3 and Al_2O_3 (**Figure 7**). The composites are equivalent to capacitors with leakage conductance. So the ac conductivities of the composites increase with increasing frequency (Figure 6b). When the reduction temperature increases to 300, 400, and 500 °C, the composites consist of Fe and Al_2O_3. Once the iron content exceeds the percolation threshold, conductive iron networks formed, leading to the metal-like conductive behavior. And the ac conductivities of the composites decrease with increasing frequency (Figure 6b–d) due to the skin effects. Besides, for samples with reduction temperature of 300 °C, σ_{ac} is almost independent of frequency at low frequencies (Figure 6b). However, for samples reduced at higher temperatures, σ_{ac} decreases with frequency in the whole tested frequency range (Figure 6c and d). As is well known, the skin depth of a conductor can be expressed as $\delta = (2/\sigma\omega\mu)^{1/2}$, where δ is the skin depth, σ is the DC conductivity, ω is the frequency, and μ is the permeability. In the present work, the effective DC conductivities σ of the composites reduced at 300 °C are lower than that of the samples reduced at 400 and 500 °C. Therefore, the skin depths δ of the samples reduced at 300 °C are larger than samples with higher reduction temperatures. That is to say, the skin effects of the samples reduced at 300 °C are too weak to result in the obvious decrease of σ_{ac} at low frequencies. However, the skin effects will become more obvious with the increase of frequency, leading to the decrease of σ_{ac} at high frequencies (Figure 6b).

Figure 8 shows the frequency dependences of ε' for the composites. We can see that negative permittivity was also obtained when the reduction temperatures were reduced to 500, 400, and 300 °C. Lower reduction temperature and lower iron content could weaken the interconnectivity of iron particles, resulting in the decrease of the negative permittivity amplitude (Figure 8b–d). However, when the reduction

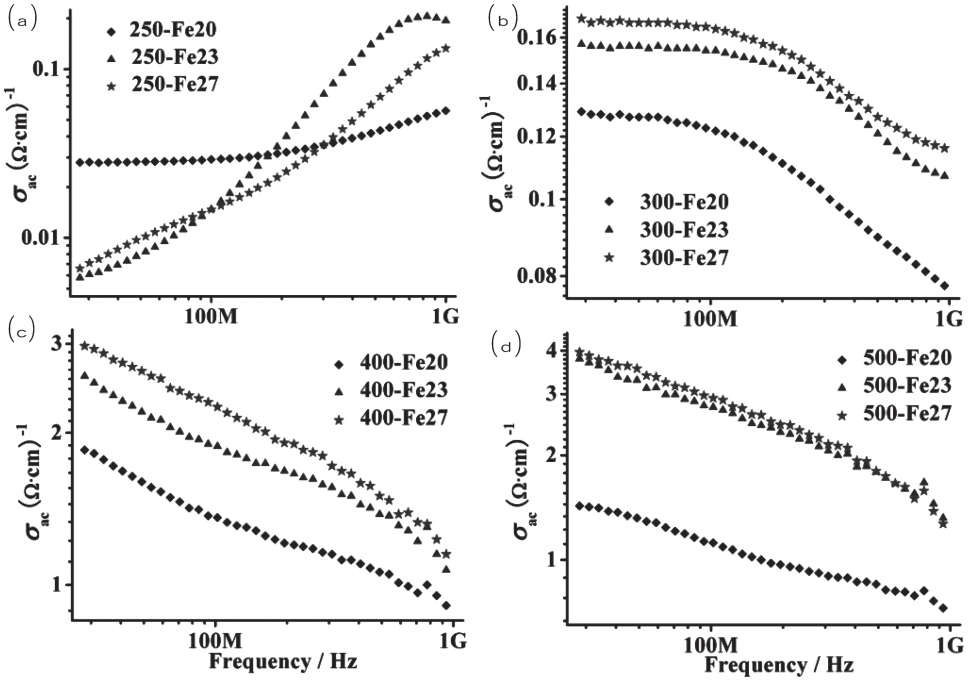

Figure 6. Frequency dependences of ac conductivity for composites prepared with different reduction temperatures.

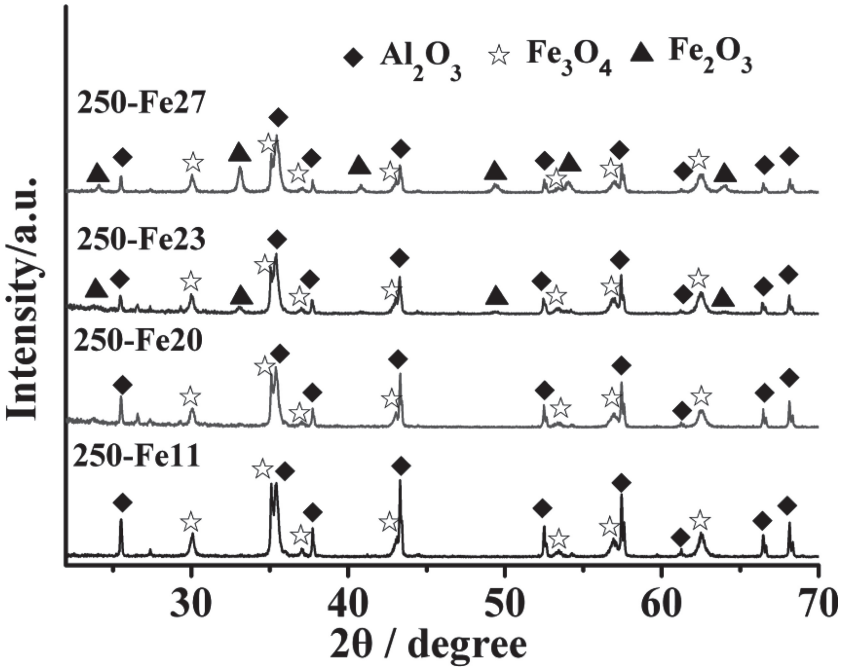

Figure 7. XRD patterns of the composites prepared with reduction temperature of 250 °C. It is indicated that when the reduction temperature was reduced to 250 °C Fe_2O_3 changed to Fe_3O_4 rather than Fe.

temperature was reduced to 250 °C, negative ε' disappeared (Figure 6a) due to the formation of Fe_3O_4 rather than Fe (XRD patterns in Figure 7). Although Fe_3O_4 is half-metallic oxide, its electron concentration is much lower than that of Fe. The low-intensity plasma oscillation of Fe_3O_4 is insufficient for the appearance of negative ε' in the tested frequency range. Besides, Fano-type resonances are also observed in Figure 8 as well as corresponding dielectric loss peaks in **Figure 9**, and the resonance peaks move to lower frequency with increasing iron content. In addition, higher reduction temperature also seems to move the resonance peaks to lower frequency. As discussed above, the resonance frequency can be expressed by $f = 1/[2\pi(LC)^{1/2}]$. The increase of iron content as well as the higher reduction temperature will enhance the interconnectivity of iron particles, leading to the increase of L. Besides, the increase of iron content will also results in larger iron-alumina interfaces, hence the increase of the effective capacitance C. Therefore, the shift of the resonance frequencies should be attributed to the increase of L and C. That is to say, the resonance frequency as well as the negative permittivity region could be controlled by the iron content and reduction temperature.

Figure 10 shows the impedance spectra of the composites with different iron contents and reduction temperatures. In this paper, iron networks were formed in porous alumina when the iron content exceeded the percolation thresholds. When the iron networks were put into a high frequency electromagnetic field, currents will be induced. And at some frequency regions, the phase of currents lags behind the phase

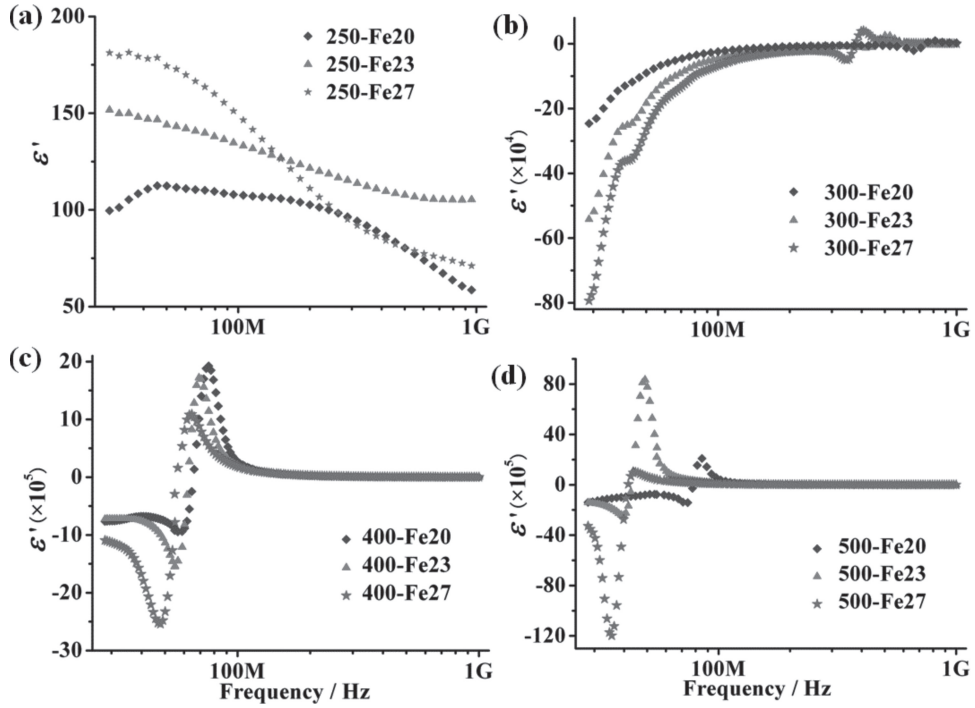

Figure 8. Frequency dependences of ε' for composites prepared with different reduction temperatures.

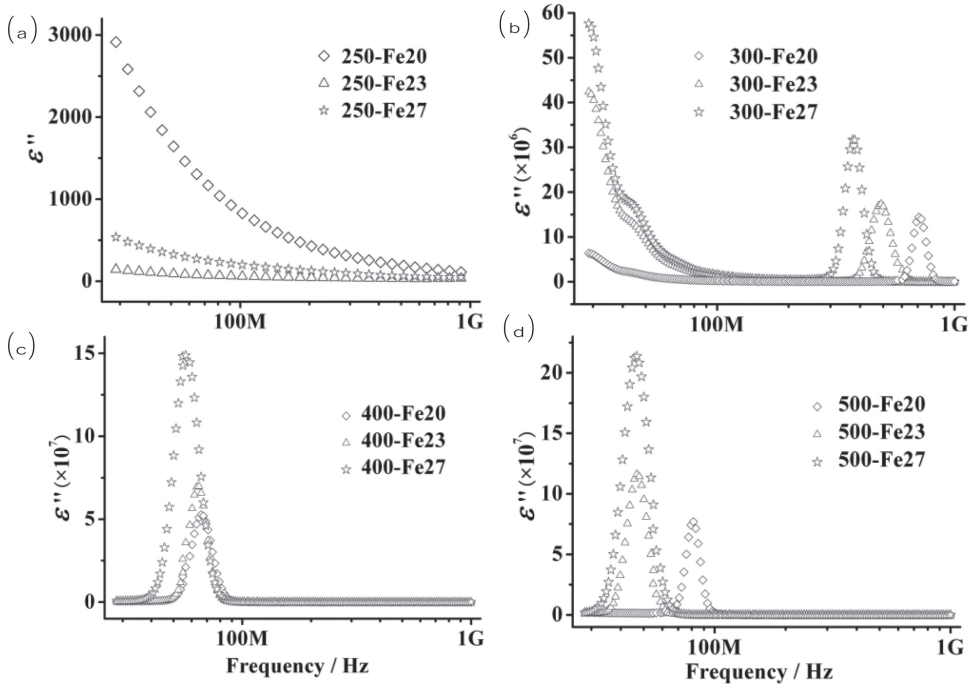

Figure 9. Frequency dependences of ε'' for composites prepared with different reduction temperatures.

of voltage, leading to the occurrence of inductive behaviors ($Z'' > 0$). As shown in Figure 10a, the composites prepared with reduction temperature of 250 °C manifests capacitive ($Z'' < 0$) behavior in the whole test frequency range. However, when the reduction temperatures are up to 300, 400, and 500 °C, the composites manifest inductive behavior at low frequency and capacitive behavior at high frequency. And the negative Z'' – positive Z'' switching frequency point (Figure 10) corresponds well to

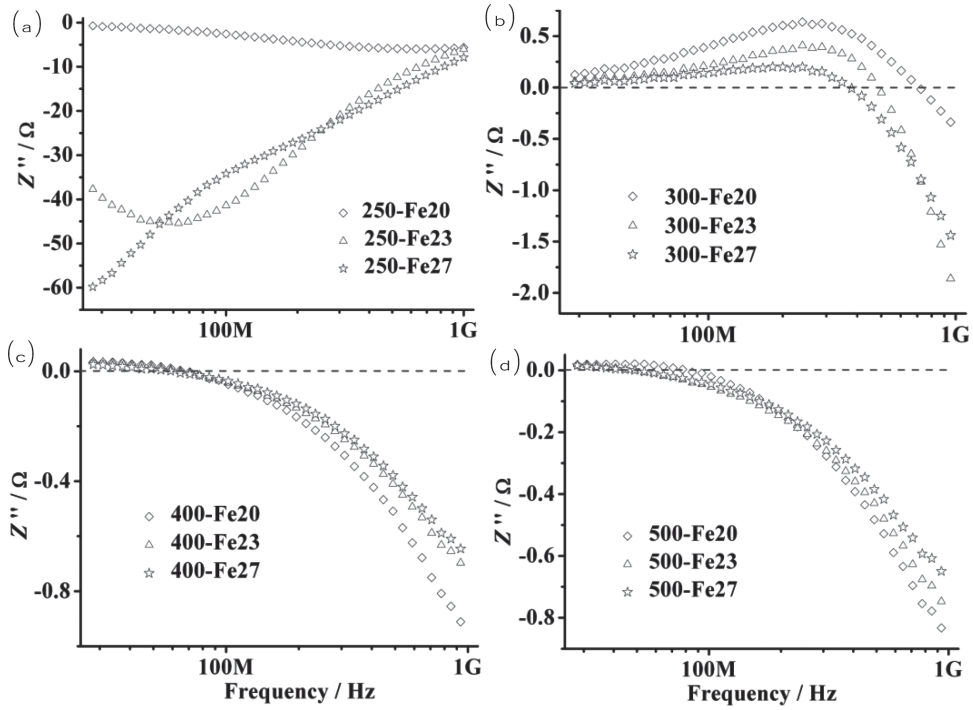

Figure 10. Frequency dependences of reactance Z'' for composites prepared with different reduction temperature.

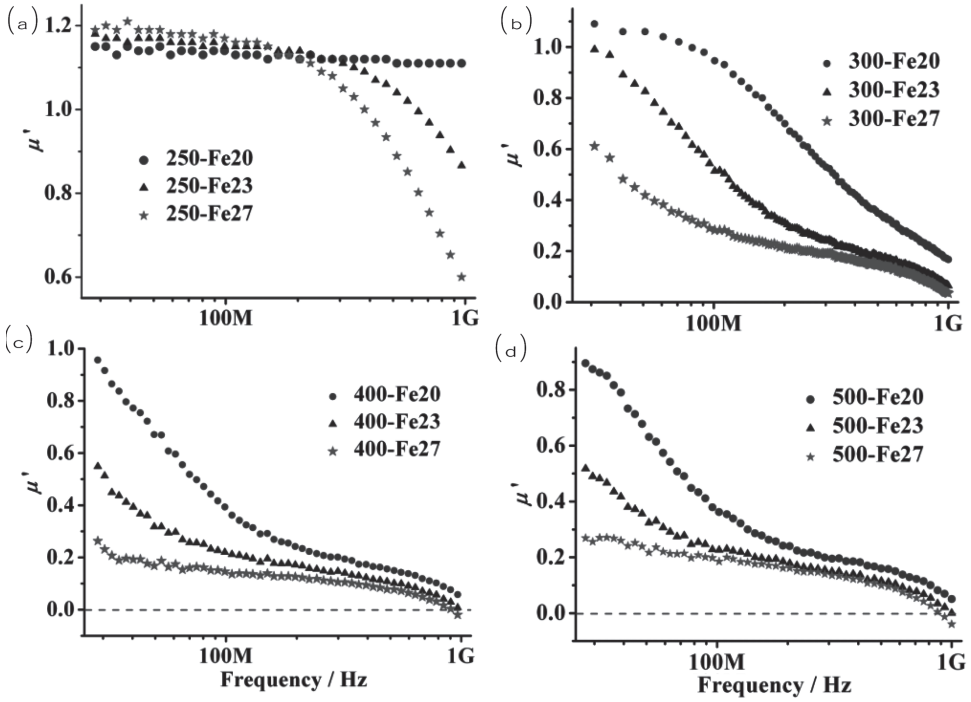

Figure 11. Frequency dependences of μ' for composites prepared with different reduction temperatures.

the positive ε' – negative ε' switching frequency point. Similar ε' - Z'' sign relationship was also observed in the Fe/Al_2O_3 composites with reduction temperature of 600 °C (Figure 4a and Figure 5d) and Ag/Al_2O_3 composites.[15]

Figure 11 shows the frequency dependences of μ' for composites prepared at different reduction temperatures. We can see that, μ' decreases with increasing frequency, and higher iron content also leads to the decrease of μ' in the tested frequency range (Figure 11b–d). As is well known, when the magnetic materials were put into a high frequency magnetic field, the magnetic losses and the eddy currents will lead to the great decrease of permeability μ'. In the present work, the magnetic losses and

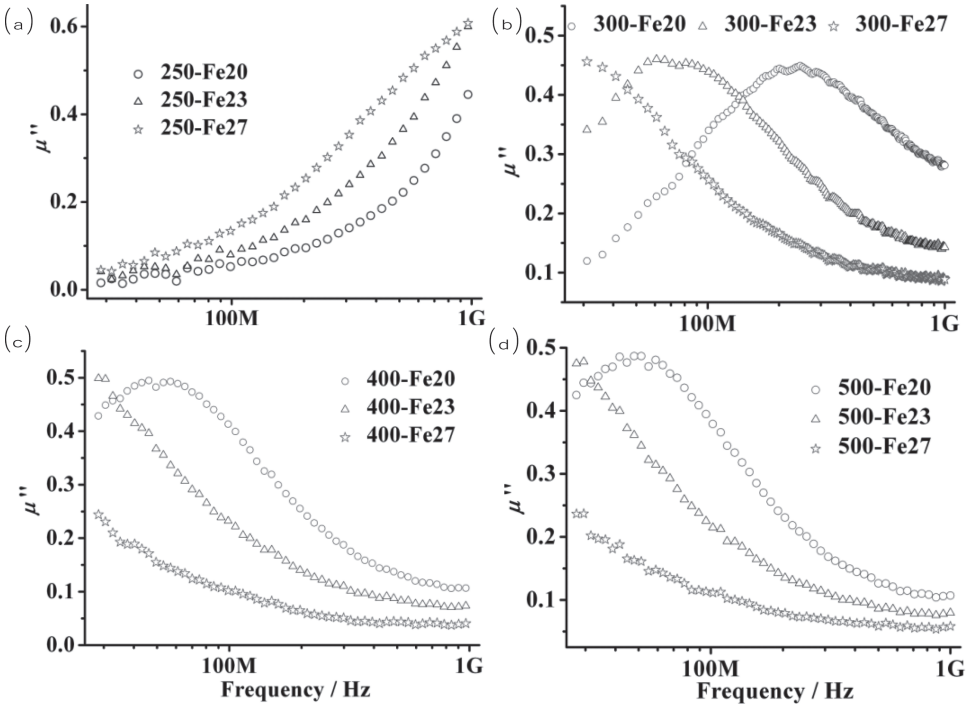

Figure 12. Frequency dependences of μ'' for composites prepared with different reduction temperatures.

eddy-current losses of the composite will increase with increasing iron content. Therefore, the μ' of the composites with higher iron content will decrease faster with frequency than composites with lower iron content. That is to say, the μ' of the composites with high iron content may be equal to or even higher than that of the composites with lower iron content at low frequencies. However, the strong magnetic losses and eddy-current losses lead to the low value of μ' in the present tested frequency range. Similar phenomenon was also reported in permalloy granular composites.[16] As shown in Figure 11c,d, negative μ' were also obtained in the high frequency when the reduction temperatures were reduced to 500 and 400 °C. Similar to the samples reduced at 600 °C, higher iron content also lead to lower μ' and broader negative μ' region. Moreover, the reduction temperature also has significant influence on the permeability spectra of the composites. For the composites with iron content of 27 wt%, the negative permeability region is 750 MHz – 1 GHz when the reduction temperature is 600 °C (Figure 4b). However, the negative permeability regions were narrowed to be 900 MHz – 1 GHz and 930 MHz – 1 GHz for composites with reduction temperature of 500 and 400 °C, respectively. Furthermore, μ' became positive in the whole test frequency range when the reduction temperature were reduced to 300 and 250 °C (Figure 11a,b). Lower reduction temperature will weaken the interconnectivity of iron particles, leading to reduced amount of current loops, hence the decrease or even disappearance of negative μ'. Therefore, the negative permeability region could be controlled by the reduction temperature and iron content. The frequency dependence of imaginary permeability spectra are shown in Figure 12. Magnetic loss peaks are observed, and these peaks move to lower frequency with increasing iron content (Figure 12b). Moreover, comparing with Figure 12b,c, we can see that for composites with the same iron content, higher reduction temperature also moves the magnetic loss peaks to lower frequency.

3. Conclusions

In summary, iron particles were hosted in porous alumina via a facile impregnation-reduction process. When the iron content exceeds the percolation threshold, the interconnectivity of iron particles results in the formation of iron networks. The composites then change from capacitive to inductive and the conductive mechanism changes from hopping conduction to metal-like conduction. The plasma oscillation of delocalized electrons in iron networks leads to negative permittivity. Meanwhile, the strong diamagnetic response of current loops in iron networks under high frequency electromagnetic field leads to negative permeability. Further investigations indicated that the iron content and reduction temperature could easily tune the amplitude and frequency range of the negative permittivity and permeability. Therefore, the impregnation-reduction process opens a new way for the realization of negative permittivity and permeability in random composites. Furthermore, the negative permittivity region and the negative permeability region could be pushed to the same frequency region by adjusting the iron content and reduction temperature. And the impregnation-reduction process has great potential for the preparation of random composites with tunable double negative property.

4. Experimental Section

The iron nitrate (99.8%, Sinopharm Chemical Reagent Co., Ltd.) was dissolved in ethanol forming 1.5 mol/L $Fe(NO_3)_3$ solution. Porous alumina discs with an open porosity of ≈60% were soaked in the solution and vacuumized for 20 min, followed by drying in an oven at 100 °C for 2 h, and calcined at 500 °C in air for 20 min. Finally, the discs were reduced in hydrogen atmosphere at 600 °C for 3 h to get the Fe/Al_2O_3 composites. Fe/Al_2O_3 composites with iron content of 11, 20, 23, and 27 wt% were prepared by repeating impregnation–heat treatment cycles. And the composites prepared with reduction temperature of 600 °C were reported as 600-Fe11, 600-Fe20, 600-Fe23 and 600-Fe27, respectively. Besides, a series of composites were further prepared with reduction temperature of 500, 400, 300, and 250 °C, and were reported as 500-Fe20, 500-Fe23, 500-Fe27, 400-Fe20, 400-Fe23, 400-Fe27, 300-Fe20, 300-Fe23, 300-Fe27, 250-Fe20, 250-Fe23, 250-Fe27, respectively. The samples were processed into square discs (15 mm × 15 mm × 2 mm) for permittivity measurements, and annular discs (inner diameter *b*, outer diameter *c* and height *h* were 6.5, 19, and 2 mm, respectively) for permeability measurements. The measurements were carried out under AC voltage 100 mV at room temperature in the frequency range from 30 MHz to 1 GHz using Agilent E4991A Precision Impedance Analyzer. And the permittivity and permeability spectra were obtained from the impedance spectra.[33] For each Fe/Al_2O_3 composite in our study, at least three samples were tested. The microstructures of the composites were investigated by scanning electron microscopy (SU-70 Field Emission Scanning Electron Microscope, FESEM).

Acknowledgements

This work was supported by National Natural Science Foundation of China (50772061, 51172131), Program for New Century Excellent Talents in University (NCET-10-518), Independent Innovation Foundation of Shandong University (GIIFSDU-YZC12076, GIIFSDU-YYX10011), and Shandong S&T Plan (2011GGX10204), 973 Project of China (2012CB825702). The Scholarship Award for Excellent Doctoral Student granted by Ministry of Education, China (31370072183613).

Received: October 5, 2012
Revised: January 8, 2013
Published online: March 15, 2013

[1] V. M. Shalaev, *Nat. Photonics* **2007**, *1*, 41.
[2] P. Alitalo, S. Tretyakov, *Mater. Today* **2009**, *12*, 22.
[3] N. Liu, H. Giessen, *Angew. Chem. Int. Ed.* **2010**, *49*, 9838.
[4] D. R. Smith, W. J. Padilla, D. J. Vier, S. C. Nemat-Nasser, S. Schultz, *Phys. Rev. Lett.* **2000**, *84*, 4184.
[5] J. F. Zhou, L. Zhang, G. Tuttle, T. Koschny, C. M. Soukoulis, *Phys. Rev. B* **2006**, *73*, 041101R.
[6] S. M. Xiao, V. P. Drachev, A. V. Kildishev, X. J. Ni, U. K. Chettiar, H. K. Yuan, V. M. Shalaev, *Nature* **2010**, *466*, 735.
[7] H. Tao, J. J. Amsden, A. C. Strikwerda, K. B. Fan, D. L. Kaplan, X. Zhang, R. D. Averitt, F. G. Omenetto, *Adv. Mater.* **2010**, *22*, 3527.
[8] T. Paul, C. Menzel, C. Rockstuhl, F. Lederer. *Adv. Mater.* **2010**, *22*, 2354.
[9] M. Beresna, P. G. Kazansky, O. Deparis, I. C. S. Carvalho, S. Takahashi, A. V. Zayats. *Adv. Mater.* **2010**, *22*, 4368.
[10] W. M. Zhu, A. Q. Liu, X. M. Zhang, D. P. Tsai, T. Bourouina, J. H. Teng, X. H. Zhang, H. C. Guo, H. Tanoto, T. Mei, G. Q. Lo, D. L. Kwong, *Adv. Mater.* **2011**, *23*, 1792.
[11] W. M. Zhu, A. Q. Liu, T. Bourouina, D. P. Tsai, J. H. Teng, X. H. Zhang, G. Q. Lo, D. L. Kwong, N. I. Zheludev. *Nat. Commun.* **2012**, *3*, 1274.

[12] A. Moreau, C. Ciracı`, J. J. Mock, R. T. Hill, Q. Wang, B. J. Wiley, A. Chilkoti, D. R. Smith. *Nature* **2012**, *492*, 86.
[13] B. Li, G. Sui, W. H. Zhong, *Adv. Mater.* **2009**, *21*, 4176.
[14] J. H. Zhu, S. Y. Wei, L. Zhang, Y. B. Mao, J. Ryu, P. Mavinakuli, A. B. Karki, D. P. Young, Z. H. Guo, *J. Phys. Chem. C* **2010**, *1142*, 16335.
[15] Z. C. Shi, R. H. Fan, Z. D. Zhang, H. Y. Gong, J. Ouyang, Y. J. Bai, X. H. Zhang, L. W. Yin, *Appl. Phys. Lett.* **2011**, *99*, 032903.
[16] T. Kasagi, T. Tsutaoka, K. Hatakeyama, *Appl. Phys. Lett.* **2006**, *88*, 172502.
[17] T. Tsutaoka, T. Kasagi, K. Hatakeyama, *J. Appl. Phys.* **2011**, *110*, 053909.
[18] A. Pimenov, A. Loidl, K. Gehrke, V. Moshnyaga, K. Samwer, *Phys. Rev. Lett.* **2007**, *98*, 197401.
[19] S. T. Chui, L. B. Hu, *Phys. Rev. B* **2002**, *65*, 144407.
[20] K. Hur, Y. Francescato, V. Giannini, S. A. Maier, R. G. Hennig, U. Wiesner, *Angew. Chem. Int. Ed.* **2011**, *50*, 11985.
[21] E. N. Economou, T. Koschny, C. M. Soukoulis. *Phys. Rev. B* **2008**, *77*, 092401.
[22] B. C. Tappan, S. A. Steiner III, Erik P. Luther, *Angew. Chem. Int. Ed.* **2010**, *49*, 4544.
[23] Z.C. Shi, R.H. Fan, Z.D. Zhang, L.Qian, M. Gao, M. Zhang, L. T. Zheng, X. H. Zhang, L.W. Yin. *Adv. Mater.* **2012**, *24*, 2349.
[24] C. Pecharromμn, J. S. Moya. *Adv. Mater.* **2000**, *12*, 294.
[25] J. C. Dyre, T. B. Schrøder, *Rev. Mod. Phys.* **2000**, *72*, 873.
[26] G. Sui, B. Li, G. Bratzel, L. Baker, W. H. Zhong, X. P. Yang, *Soft Matter* **2009**, *5*, 3592–3598.
[27] C. H. Hsieh, A. H. Lee, C. D. Liu, J. L. Han, K. H. Hsieh, S. N. Lee, *AIP Adv.* **2012**, *2*, 012127.
[28] D. Y. Zhang, P. P. Wang, R. Murakami, X. P. Song, *Appl. Phys. Lett.* **2010**, *96*, 233114.
[29] S. Basu, D. Chakravorty, *J. Non-Cryst. Solids* **2006**, *352*, 380–385.
[30] J. B. Pendry, A. J. Holden, W. J. Stewart, I. Youngs, *Phys. Rev. Lett.* **1996**, *76*, 4773–4776.
[31] T. Kasagi, T. Tsutaoka, K. Hatakeyama, *J. Appl. Phys.* **1997**, *82*, 3068–3071.
[32] Y. Poo, R. X. Wu, G. H. He, P. Chen, J. Xu, R. F. Chen, *Appl. Phys. Lett.* **2010**, *96*, 161902.
[33] *Agilent Impedance Measurement Handbook(5950-3000)*, Agilent Technologies, USA **2009**, p. 8–10.